

PAPER

View Article Online
View Journal | View Issue



Cite this: *Environ. Sci.: Water Res. Technol.*, 2021, 7, 1873

Amyloid fibril-based membranes for PFAS removal from water†

Tonghui Jin,^a Mohammad Peydayesh,^{iD}^a Hanna Joerss,^{bc} Jiangtao Zhou,^a Sreenath Bolisetty^d and Raffaele Mezzenga^{iD}^{*ae}

We introduce a green and efficient approach for removing per- and polyfluoroalkyl substances (PFASs) based on the β -lactoglobulin amyloid fibril membrane. The membrane exhibits superior adsorption capability for long-chain PFASs. At low pH, the membrane efficiency improved significantly due to enhanced electrostatic interactions between positively charged fibrils and negatively charged PFASs. Furthermore, intermolecular adhesion force measurements confirm the hydrophobic–hydrophobic interaction at the nanoscale with PFOS and PFOA representing perfluoroalkyl sulfonic acids (PFSA) and perfluoroalkyl carboxylic acids (PFCAs), respectively. For real PFAS-contaminated water from the Xiaoqing River basin and under single-step filtration mode, the membrane exhibits high efficiency for removing both high ($> \mu\text{g L}^{-1}$) and trace (ng L^{-1}) levels of the compounds. To demonstrate the scalability and generality, a commercial amyloid–carbon-based hybrid membrane is applied for removal of a range of long-chain and short-chain PFASs as well as their replacement compounds, offering complete removal of PFASs with ≥ 4 perfluorinated carbon atoms in the molecular structure and a removal efficiency of low molecular weight PFBA (3 perfluorinated carbon atoms) exceeding 96%. Analysis of the sustainability footprint reveals the superiority of the amyloid–carbon hybrid membrane for PFAS removal. Altogether, these results demonstrate a high potential of amyloid fibril membrane technology for the sustainable removal of PFASs from water.

Received 2nd June 2021,
Accepted 16th August 2021

DOI: 10.1039/d1ew00373a

rsc.li/es-water

Water impact

We introduce a technology based on protein nanofibrils and porous carbon allowing removal of per- and polyfluoroalkyl substances (PFASs) from water at efficiencies exceeding 96% in real water samples and with a sustainability footprint superior to that of current technologies.

Introduction

Certain PFASs, also known as “forever chemicals”, are listed as persistent organic pollutants (POPs) under the Stockholm Convention due to their ubiquity, persistence, toxicity, and bio-accumulative nature in the environment.¹ Health concerns of the various kinds of PFASs are controversial, and there are still many uncertainties regarding the exact toxicity and damage to the environment and the human body. For

instance, a study involving 69 000 individuals from the surroundings of a manufacturing plant in the United States found that there was a probable link between perfluorooctanoic acid (PFOA) exposure and at least six diseases: kidney cancer, testicular cancer, thyroid disease, ulcerative colitis, high cholesterol, and pregnancy-induced hypertension.¹ PFASs can be found not only in industrial products but also in contaminated human blood, breast milk, and umbilical cord blood.² PFASs have already been found in low ng L^{-1} levels in aquatic environments and different water sources, such as lakes, rivers, tributaries, and groundwater.^{3–5}

By considering the potential effects on the environment and human health, various techniques have been used to remove PFASs from water. Application of conventional technologies, such as oxidation, photocatalysis and sonochemistry, is not economical and energy-efficient for treating a large volume of contaminated water with trace concentrations of PFASs.⁶ Moreover, the concentration of PFASs is typically much lower (several orders of magnitude) than that of the background

^a Department of Health Sciences and Technology, ETH Zurich, 8092 Zurich, Switzerland. E-mail: raffaele.mezzenga@hest.ethz.ch

^b Helmholtz-Zentrum Hereon, Institute of Coastal Environmental Chemistry, Max-Planck-Str. 1, 21502 Geesthacht, Germany

^c Institute of Inorganic and Applied Chemistry, Universität Hamburg, Martin-Luther-King-Platz 6, 20146 Hamburg, Germany

^d BluAct Technologies GmbH, Dufaux-strasse 57, 8152 Zurich, Switzerland

^e ETH Zurich Department of Materials, Wolfgang-Pauli-Strasse 10, 8093 Zurich, Switzerland

† Electronic supplementary information (ESI) available. See DOI: 10.1039/d1ew00373a



components, which makes it difficult for conventional technologies to be scaled up for industrial applications. Adsorption-based technologies, such as activated carbon, minerals, polymers, and ion exchange resins, have been extensively used in lab-scale investigation and large-scale practical applications.⁷ However, a few drawbacks emerge in some specific applications despite their performance. For example, the adsorbents are usually in the form of granules or powder, making it challenging to recover them from the water after use.^{6,8} Additionally, the release of certain components such as carbon nanotubes (CNTs) may cause a risk of secondary pollution in the water environment.⁹ The combination of adsorption and membrane technology can effectively overcome these shortcomings, and the adsorbents can be easily separated and replaced after saturation.

Amyloid fibril-based purification technology has demonstrated superior performance in removing contaminants from wastewater.^{10–16} For example, the membranes showed a remarkable ability to treat polluted water, such as toxic heavy metal ions and nuclear waste, due to their strong metal-binding interactions.¹¹ Additionally, arsenic has also been removed efficiently from contaminated water in a cost-effective way, regardless of the oxidation state of the arsenic.¹² As a bio-based membrane generated from the very inexpensive whey protein (cheese industry by-product), it provides a green approach compared to traditional technologies to meet the water pollution crisis. However, to date, this outstanding hybrid membrane has not yet been considered in the context of PFASs.

Here, we report the application of amyloid fibril-based membranes for universal PFAS treatment and show that the adsorption performance relies on the synergy between the amyloid properties and the molecular traits of PFASs. We firstly test a broad range of PFASs, including long- and short-chain PFCAs and PFSAs and their precursors as well as their replacement and overlooked compounds. The study is further designed to also investigate the electrostatic interaction by adjusting the pH. Force-distance based atomic force microscopy (FD-AFM) is applied to examine the attractive interaction between amyloid fibrils and two representatives (PFOS and PFOA). We finally benchmark amyloid fibril performance against that of real industrial effluents in the Xiaoqing River basin and further examined the performance of a commercial amyloid-carbon hybrid membrane for comprehensive PFAS treatment.

Materials and methods

Chemicals and reagents

BioPURE β -lactoglobulin was purchased from the Technische Universität Munich, Department of Food Process Engineering and Dairy Technology, Munich, Germany. For more information on the purification of β -lactoglobulin and the detailed preparation of amyloid fibrils, see ref. 17. BluAct Technologies GmbH kindly provided the commercial amyloid-carbon hybrid membrane. 31 target PFAS analytes (for chemical information, see the ESI[†] Tables S1 and S2) were used for spiking MilliQ

water: 11 PFCAs (C₄ to C₁₄), five PFSAs (C₄, C₆, C₇, C₈, and C₁₀), the cyclic PFAS PFECHS, six per- and polyfluoroalkyl ether carboxylic and sulfonic acids (PFECAs and PFESAs, *i.e.*, HFPO-DA, HFPO-TrA, HFPO-TeA; DONA; 6:2 and 8:2 Cl-PFESA), two perfluoroalkyl phosphinic acids (PFPIAs, *i.e.*, 6:6 PFPIA and 6:8 PFPIA), six precursors (*i.e.*, FOSA; 4:2 FTSA, 6:2 FTSA, 8:2 FTSA, N-EtFOSE, and N-EtFOSAA). A total of 13 mass-labeled internal standards (IS) was used, which included seven isotopically labeled PFCAs (¹³C₄-PFBA, ¹³C₂-PFHxA, ¹³C₄-PFOA, ¹³C₅-PFNA, ¹³C₂-PFDA, ¹³C₂-PFUnDA, and ¹³C₂-PFDoDA), three PFSAs (¹³C₃-PFBS, ¹⁸O₂-PFHxS, and ¹³C₄-PFOS), one PFECA (¹³C₃-HFPO-DA) and two precursors (¹³C₂-6:2 FTSA and ¹³C₈-FOSA). ¹³C₈-PFOA was used as the injection standard. For detailed information on the target analytes and the standards' purity and concentration, see ref. 18.

Characterization of amyloid fibril-based membranes

The permeability (L m⁻² h⁻¹ bar⁻¹) was determined by collecting the volume of the permeated water (*V*, L) for a certain period (*t*, h) at unit membrane area (*A*, m²) and unit operation pressure (*P*, bar) as:

$$\text{Permeability} = \frac{V}{A \times t \times P} \quad (1)$$

where *A* is determined by a filter with 15 mm diameter.

The observed removal rate (*R*, %) was defined as follows:

$$R = \left(1 - \frac{C_p}{C_f}\right) \times 100\% \quad (2)$$

where *C_f* and *C_p* are the bulk feed concentration and permeate concentration, respectively.

Preparation of pure amyloid fibril membranes

Pure amyloid fibril membranes were prepared to treat PFAS-spiked MilliQ water. Typically, amyloid fibrils are obtained from denatured β -lactoglobulin at pH 2 and high temperature (90 °C) in 5 hours. To yield a pure protein fibril membrane, 10 ml of a 0.2 wt% dispersion of protein fibril solution was vacuum-filtered using 0.22 μ m cellulose acetate (CA) filters (diameter, 40 mm). The extreme adhesiveness and stiffness of the protein fibrils enabled the homogeneous assembly of the amyloid fibril adsorption membranes onto the substrate filter. After rinsing with 5 ml MilliQ water, these adsorption membranes were then used to filter PFAS-spiked MilliQ water.

Binding isotherms and adsorption capacity

To evaluate binding isotherms, fixed concentrations of amyloid fibril solution (2.5 mL of 2 wt%) were titrated using various PFOS and PFOA concentration ranges having a final volume of 15 mL. After 24 h of equilibrium time, the solutions were filtered using a cellulose support membrane with a pore size of 0.22 μ m. The concentration of PFASs (PFOS or PFOA) in the permeate was measured again, and by difference, the adsorbed amount was calculated using eqn (3):



$$q_e = \frac{C_i - C_e}{W} \times V \quad (3)$$

in which C_i and C_e stand for PFAS (PFOS or PFOA) concentrations before and after adsorption ($\mu\text{g L}^{-1}$), respectively. W stands for the adsorbent weight (g). V stands for final volume (L).

All experiments were repeated three times, and the mean values and errors were reported. Then, the approach of Swillens¹⁹ and Motulsky²⁰ was applied to fit the binding isotherms. A single binding PFAS (PFOS and PFOA)–ligand pair with a single, average, binding constant is assumed in this approach:

$$[M \cdot L] = \frac{1}{2} \left([M_0] + [L_0] + \frac{1}{K_a} \right) - \frac{1}{2} \sqrt{\left([M_0] + [L_0] + \frac{1}{K_a} \right)^2 - 4[M_0][L_0]} \quad (4)$$

in which $[M]$ and $[L]$ are the bound PFASs (PFOS or PFOA) and ligand concentrations (identical to $[M \cdot L]$), $[M_0]$ and $[L_0]$ are the initial total PFASs (PFOS or PFOA) and ligand concentrations, respectively, and K_a is the binding constant.

Intermolecular adhesion force measurements and analysis

To investigate the adhesion force between PFASs and amyloid fibrils, a silicon AFM probe (RTESPA-150) was utilized, but two different approaches were prepared to immobilize PFOS and PFOA on the AFM tip. For PFOS, the probe was first coated with a thin layer of gold (10 nm) and then immersed in a $1 \mu\text{g L}^{-1}$ PFOS solution for 1 min. With the bonding between the gold surface and the thiolated end of PFOS, the C–F hydrophobic tails are exposed and interact with amyloid fibrils during the measurement. For PFOA, first, we treated the probe in an ozone cleaner for 10 min and then functionalized it by immersing it in 1% (3-aminopropyl) triethoxysilane (APTES) to expose the amine group on the tip and then dried by a gentle flow of compressed air. After that, the probe was immersed in $1 \mu\text{m mL}^{-1}$ PFOA solution for 1 min to immobilize PFOA by interacting with the exposed amine group of APTES on the tip.^{21–23}

Aliquots of amyloid fibril solution at a concentration of 0.02 wt% were deposited on freshly cleaved mica for 2 min and dried by a gentle airflow after a smooth rinse. The intermolecular adhesion force was measured using the PeakForce tapping mode of the AFM (Nanoscope Multimode 8, Bruker, Santa Barbara, USA). During AFM mapping measurement, the information of both morphology and adhesion, as well as several force–distance curves during the approaching and extracting process were recorded. First, a bare AFM tip was used before each measurement, and then the functionalized probe was applied for the same measurement. Image processing and data analysis were performed using the Nanoscope analysis software.

Sample analysis

The real water sample was collected at a depth of 0.5 m from the surface of the river. Before measuring the sample, glass

microfiber filters (Whatman, grade: GF/F, pore size: 0.7 mm, diameter: 47 mm, GE Healthcare, USA) were used for filtration of the samples after baking the filters at 450 °C in a muffle furnace overnight. For analysis of samples from the pure amyloid fibril membrane, the detailed processes are discussed in ref. 18. In brief, a sample of 25 mL was concentrated using solid-phase extraction (SPE) and then analyzed using an HP 1100 LC system (Agilent Technologies, USA) coupled to an API 4000 triple quadrupole mass spectrometer (AB Sciex, USA). It was equipped with a Turbo V ion source (AB Sciex, USA) operating in negative electrospray ionization mode. Chromatographic separation was achieved on a polar embedded reversed phase C18 separation column (Synergi Fusion-RP C18, Phenomenex, USA). As solvents for the gradient elution, 2 mM ammonium acetate aqueous solution (A) and 0.05% acetic acid in methanol (B) were used. The injection volume was 10 μL for samples and standards, both dissolved in 80:20 (v/v) methanol/water. The internal standard method was used for quantification of the target analytes, and quality control is always considered during the measurement processes. For detailed information, see ref. 18. For the analysis of samples from the amyloid–carbon hybrid membrane, the results are provided by Trident Laboratories with the EPA Method 537 M.

Results and discussion

Amyloid fibril membrane for PFAS adsorption

We first investigated PFAS removal by pure amyloid fibril (AM) membranes. The AM membrane was simply prepared by vacuum-assisted filtration of 10 ml of a 0.2 wt% protein fibril solution. Before PFAS filtration, the feed MilliQ water was spiked with 31 PFASs (400 ng L^{-1} each) to match typical trace-level contaminated water values. These PFASs were grouped as PFCAs and PFASs, replacement PFASs, overlooked PFASs, and precursors.

Fig. 1 shows the filtration performance of the AM membrane while CA supports the membrane and also serves as blank control. The permeability of the cellulose acetate membrane, pure amyloid membrane, and amyloid–carbon hybrid membrane is 7114.0 ± 280.0 , 301.8 ± 32.7 , and $1738.9 \pm 176.5 \text{ L m}^{-2} \text{ h}^{-1} \text{ bar}^{-1}$, respectively (as shown in Fig. S1†). These values are in the range for those of microfiltration or ultrafiltration, corresponding to the molecular weight cut-off (MWCO) of 10–1000 kDa. However, the maximum molecular weight of PFAS measured in this study was 824.06 Da (6:8 PFPIa), which is much smaller than the MWCO of the membranes. Hence, the effect of pore size, in this case, can be neglected.

At the neutral pH of feed water, the presence of amyloid fibrils on the CA support membrane (as an adsorbent) decreases the concentration of PFASs in the permeate. This is predominantly due to the adsorption by amyloid fibrils. The concentrations of PFTrDA (MW 664 Da) and PFTeDA (MW 714 Da) in the permeate treated by AM membrane were lower than 70 ng L^{-1} at neutral pH and reached the EPA guideline



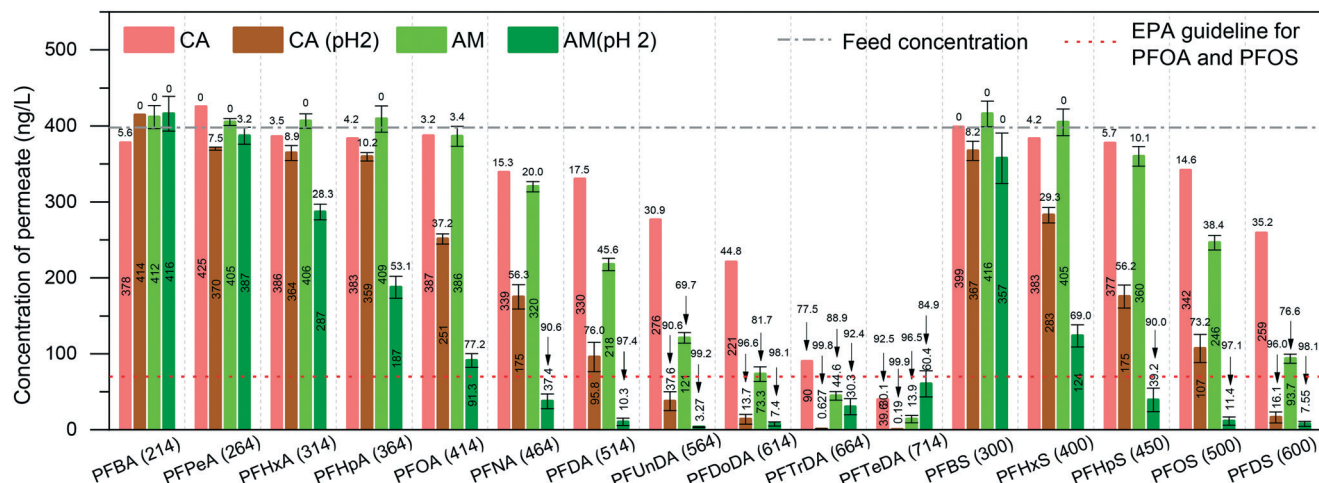


Fig. 1 Concentrations of PFCAs and PFSA in the permeate. The pH of the feed is around 7 unless otherwise stated. The number in the brackets is the MW of each compound. The red dashed line stands for EPA guideline for PFOA and PFOS regulation, which is 70 ng L⁻¹. The grey dashed line stands for the spike concentration of each PFAS, which is around 400 ng L⁻¹. The removal efficiencies (%) are shown above the permeate bars.

of PFOS and PFOA. However, the mechanism is a complex adsorption process. Therefore, to determine the dominant mechanism between physisorption and chemisorption, we adjusted the pH of the feed to 2, where the amyloid fibrils have a higher positively charged density, to investigate the removal performance. The concentration of the permeate was reduced dramatically by both the CA and the AM membrane at pH 2. The PFCAs and PFSA are strong acids with low pK_a values in a wide range of pH, including neutral pH, and therefore they will be in their ionic state.^{24,25} Moreover, the membrane surface charge is set by the amyloid fibrils since the protein fully covers the CA support membrane. The isoelectric point of BLG amyloid fibrils is around 5, which means that the pure amyloid fibrils are negatively charged at pH 7 and positively charged at pH 2.^{26–28} These indications suggest that PFASs may undergo electrostatic adsorption onto proteins whose surface charge is positive at pH values below the isoelectric point (\sim pH 5).^{26,27} Additionally, to further increase the electrostatic interaction between amyloid fibrils and PFASs, it is possible to activate the amyloid fibril membrane by rinsing with acidic water to provide the membrane with a higher charge density.

A clear shift of removal rate as a function of PFAS MW can be observed when the pH dropped to 2 (shown in the ESI,† Fig. S2). The lowest MW of PFASs, for which the permeate concentration meets the EPA guideline of PFOA and PFOS, shifted from MW 664 Da (PFTTrDA) to MW 450 Da (PFHpS) at pH 2. This also confirms that the increase of the charge density of amyloid fibril provides a strong electrostatic force at low pH.

Long-chain PFASs are more easily adsorbed than short-chain ones. Fig. 1 shows that the removal rate increases along with the chain length of both PFCAs and PFSA. This phenomenon is in good agreement with the other related reports.^{29–31} Long-chain PFASs with a larger number of C–F units are more hydrophobic than the short-chain ones, leading to higher hydrophobic interaction by amyloid

fibrils.^{32–34} Meanwhile, the short-chain PFASs are more soluble, and the effect of hydrophobicity decreases significantly.

We also measured the removal performance of replacement PFASs and overlooked PFASs as well as precursors to PFCAs and PFSA (for chemical information, see the ESI,† Table S2). Among the alternatives, hexafluoropropylene oxide (HFPO) oligomers are the replacement for PFOA in many cases and have globally been found in waters.^{35–37} The removal performance of HFPO-DA, HFPO-TrA, and HFPO-TeA (Fig. 2) shows that the concentration of permeate decreases with the increase of molecular size of HFPO (HFPO-TeA > HFPO-TrA > HFPO-DA). It has been found that the protein–PFAS reaction was predominantly driven by hydrophobic interaction.³⁸ This indicates that a molecule with more C–F units is easily absorbed by amyloid fibrils, where the increased hydrophobicity plays the dominant role in the adsorption, compared to molecules with less C–F units. Furthermore, the same trend can be found on 6:2 Cl-PFESA and 8:2 Cl-PFESA, 6:6 PFPIA and 6:8 PFPIA, and (4:2, 6:2) FTSA and 8:2 FTSA.

On the other hand, the ratio of C–F units within the molecule affects the removal performance. For instance, PFOS and 6:2 FTSA, shown in Fig. 1 and 2, have the same carbon bond in their molecular chain, while the major difference is the number of perfluoroalkyl moieties (8 C–F units for PFOS and 6 C–F units for 6:2 FTSA). At pH 2, the concentration of PFOS in the permeate is 11.4 ng L⁻¹, but the concentration of 6:2 FTSA in the permeate is around 112 ng L⁻¹, which is higher than the EPA guideline (70 ng L⁻¹). Moreover, PFECHS, also known as cyclic PFOS, has 8 carbon atoms in its molecular structure, which is the same as that of PFOS. The cyclic structure reduces two fluorine atoms and shortens the length of the molecule (see the ESI,† Table S2), which leads to a weaker binding affinity of PFECHS on the amyloid fibrils than the PFOS.



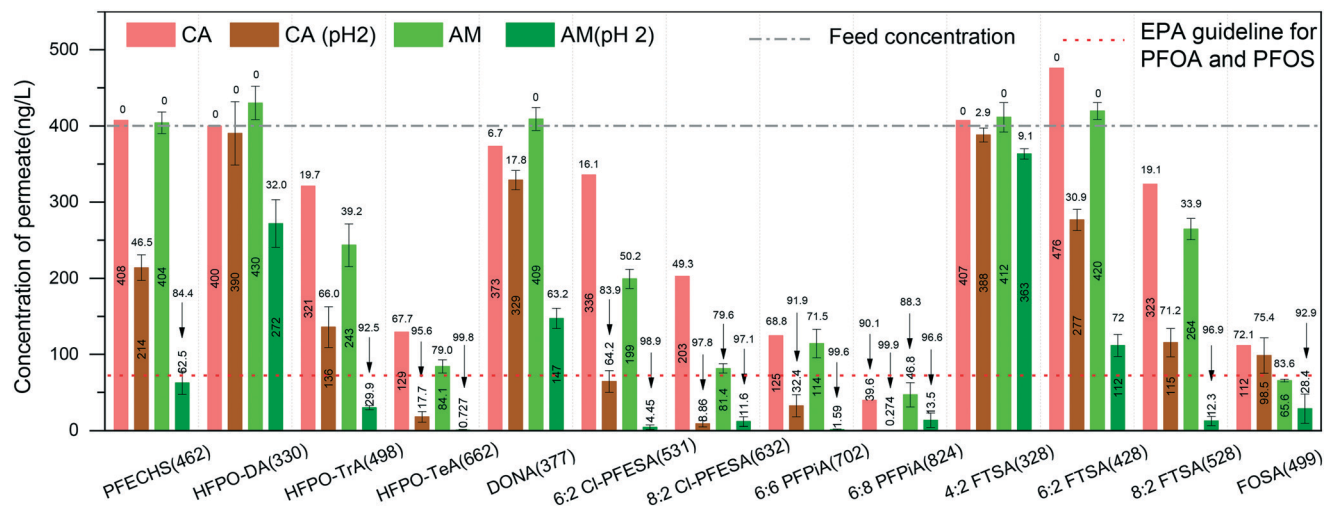


Fig. 2 Concentrations of replacement PFASs and overlooked PFASs in the permeate (PFAAs). The pH of the feed is around 7 unless otherwise stated. The number in the brackets is the MW of each compound. The red dashed line stands for the EPA guideline for PFOA and PFOS regulation, which is 70 ng L⁻¹. The grey dashed line stands for the spike concentration of each PFAS, which is around 400 ng L⁻¹. The removal efficiencies (%) are shown above the permeate bars.

Adsorption isotherm and intermolecular adhesion forces

In our previous work we performed adsorption isotherms on a model system between amyloid fibrils and heavy metals, which provided insight into the binding process.³⁹ Here, PFOS and PFOA were chosen to investigate the binding isotherms by changing their concentrations at a fixed concentration of amyloid fibrils. The fitted binding isotherm for PFOS and PFOA is shown in Fig. 3. The results show that the saturation limit of PFOS is 157 μ M, which is lower than that of PFOA (456 μ M). However, the binding constant of PFOS (2523 M⁻¹) is larger than that of PFOA (900 M⁻¹), which means that the adsorption affinity of PFOS is more favorable than that of PFOA. The possible reason could be that PFOS has more CF₂ units than PFOA, leading to enhanced attractive hydrophobic interactions. These results have

demonstrated that PFOS is more easily adsorbed while PFOA has a higher saturation limit per amount of absorbent.

To further confirm the role of hydrophobic interaction in the interaction of PFASs (PFOS, PFOA) and amyloid fibrils, we explored their adhesive interaction at a single-molecule scale by employing AFM force spectroscopy as quantitative assessment. AFM is a powerful tool and has been widely used to measure a series of nanoscale interaction forces in various applications such as protein unfolding and membrane protein as well as membrane fouling research.^{40,41} Elimelech *et al.* demonstrated that AFM can measure the intermolecular adhesion force in foulant-membrane and foulant-foulant pairs.^{42,43} Here we have measured the intermolecular adhesion force by carrying out AFM force spectroscopy with PFAS-functionalized AFM tips on amyloids fibrils.



Fig. 3 Fitted binding isotherm of PFOS and PFOA.

The AFM images show the morphology of the amyloid fibril and the adhesion map between AFM tips and amyloid fibrils, in the case of PFOS (Fig. 4a) and PFOA (Fig. 4b). Each pixel on the AFM morphological images represents a circle of AFM probe approaching and retracting from the amyloid fibrils, recorded as force-distance (FD) curves. The adhesive interaction between PFASs and amyloids was extracted from the force-distance curves, specifically the minima of the retracting curve.

Comparing the adhesion map before (blue boxes) and after (red boxes) PFAS functionalization, we could notice larger adhesion forces (*i.e.*, more negative values) on the amyloid surface when using PFAS-coated AFM cantilevers compared to the bare tip. This indicates that the interaction increased when PFAS molecules mediate the interaction of the tip with the amyloid fibrils.

The FD curves in Fig. 4c and d, extracted from the adhesion maps on the region of the amyloid fibril in Fig. 4a and b, show that the PFOS and PFOA functionalized tips exhibit higher adhesion forces (red curve) than the virgin tips (blue curve). Statistical adhesion force analysis of FD curves on the amyloid fibrils at 30 different locations is summarized in Fig. 4e and f. A dramatic enhancement of the adhesive force was measured between the functionalized and virgin tip cases, specifically increasing from 3 nN to 6 nN and from 2 nN to 7 nN for modification of the tip with PFOS and PFOA, respectively. We infer that this adhesive interaction is dominated by hydrophobic interactions between the C-F chain of PFOS and PFOA and hydrophobic amino groups of amyloid fibrils, since the ionic groups of PFASs are used to attach the PFASs to the tip and are no longer available to contribute to electrostatic adhesion to the amyloid surface.

Real water treatment

River water samples were collected downstream of an industrial point source in the Chinese Xiaoqing River basin (Huantai, Shangdong Province), where one of the largest Asian fluoropolymer production sites is located (for sample information, see the ESI† Table S3). Its main products are polytetrafluoroethylene (PTFE), vinylidene fluoride (VDF), fluoroelastomers (FKM), and polyvinylidene fluoride (PVDF).⁴⁴ Due to the limited phase-out of long-chain PFCAs, short-chain compounds did not dominate the contamination near the site. Therefore, PFOA is still the most prevalent substance of the detected target analytes, contributing approximately 80% to \sum PFASs.

Fig. 5 shows the real water treatment through single-step filtration by the pure amyloid membrane. The PFOA concentration decreases from 327 $\mu\text{g L}^{-1}$ to 241 $\mu\text{g L}^{-1}$. The removal of PFOA is a dynamic adsorption process by amyloid-based membranes; the apparent adsorption capacity is still above the saturation limits of these membranes.

Furthermore, there are other pollutants in water in real conditions that can be adsorbed by amyloid fibrils, decreasing the number of active sites for adsorbing PFASs. On the other hand, the real water contaminated with PFASs is alkaline, at which the amyloid-based membrane is negatively charged, which reduces the electrostatic interaction between negatively charged PFASs and amyloid fibrils.

The removal efficiency of long-chain HFPO-TrA is higher than 90%, consistent with the previous conclusion about the treatment of PFAS-spiked water. Again, the membrane shows the ability to remove trace PFNA and reduces the concentration of PFNA from 51.65 ng L^{-1} (feed water) to 14.31 ng L^{-1} (permeate water). It displays better performance than treating PFAS-spiked water. The possible reason may be the increased hydrophobicity of the membrane after the quick saturation by the adsorbed PFAAs, which further enhances the overall hydrophobic interaction. Moreover, some reports confirm that organic compounds, such as humic acid, facilitate the removal of PFASs by nanofiltration/RO *via* forming organic/inorganic ion-PFAS complexes larger than the membrane pore size.^{45,46} On the other hand, the weak removal performance of short-chain PFASs, such as PFBA, PFPeA, PFHxA, PFHpA, and HFPO-DA, is predictable and consistent with the previous conclusions on the performance for low-molecular-weight PFASs.

Amyloid-carbon hybrid membrane

Short-chain PFASs are more persistent and mobile in aquatic systems. In general, it is particularly challenging to remediate short-chain PFASs, for which efficient treatment methods are quite limited in the current literature. A nanofiltration membrane is efficient in removing long-chain PFASs (removal rate: 85–99%) but weak in rejecting short-chain PFASs (removal rate: 20–70%).⁴⁷ A reverse osmosis membrane, in general, has higher efficiency in removing both long- and short-chain PFASs, which can reach 99% but at the expense of significant energy consumption.^{48,49} Moreover, weak removal efficiencies of short-chain PFASs were reported on many adsorbents, such as ion-exchange resins (11–90%), biochar (the adsorption of PFBA is 75% lower than that of PFOA), synthetic materials (*e.g.* MWCNTs: 30%), *etc.*^{50–52} Thus, there is still an urgent need to promote new technologies for short-chain PFAS removal.⁵³

In our earlier reports, we demonstrated a series of hybrid amyloid fibril membranes for removing efficiently a broad spectrum of heavy metal ions^{11,12} as well as fluoride,⁵⁴ organic compounds,⁵⁵ and radioactive wastewater efficiently.¹³ Therefore, to improve the performance of the AM membrane for short-chain PFAS remediation, we naturally turn to the same amyloid-carbon hybrid membrane. The feed sample and permeate sample were measured under the EPA Method 537 M. Before filtration, the concentrations of compounds were higher than the EPA guidelines for PFOS and PFOA (shown in Fig. 6, only PFHxS is a bit lower than 70 ng L^{-1}). The results show that the



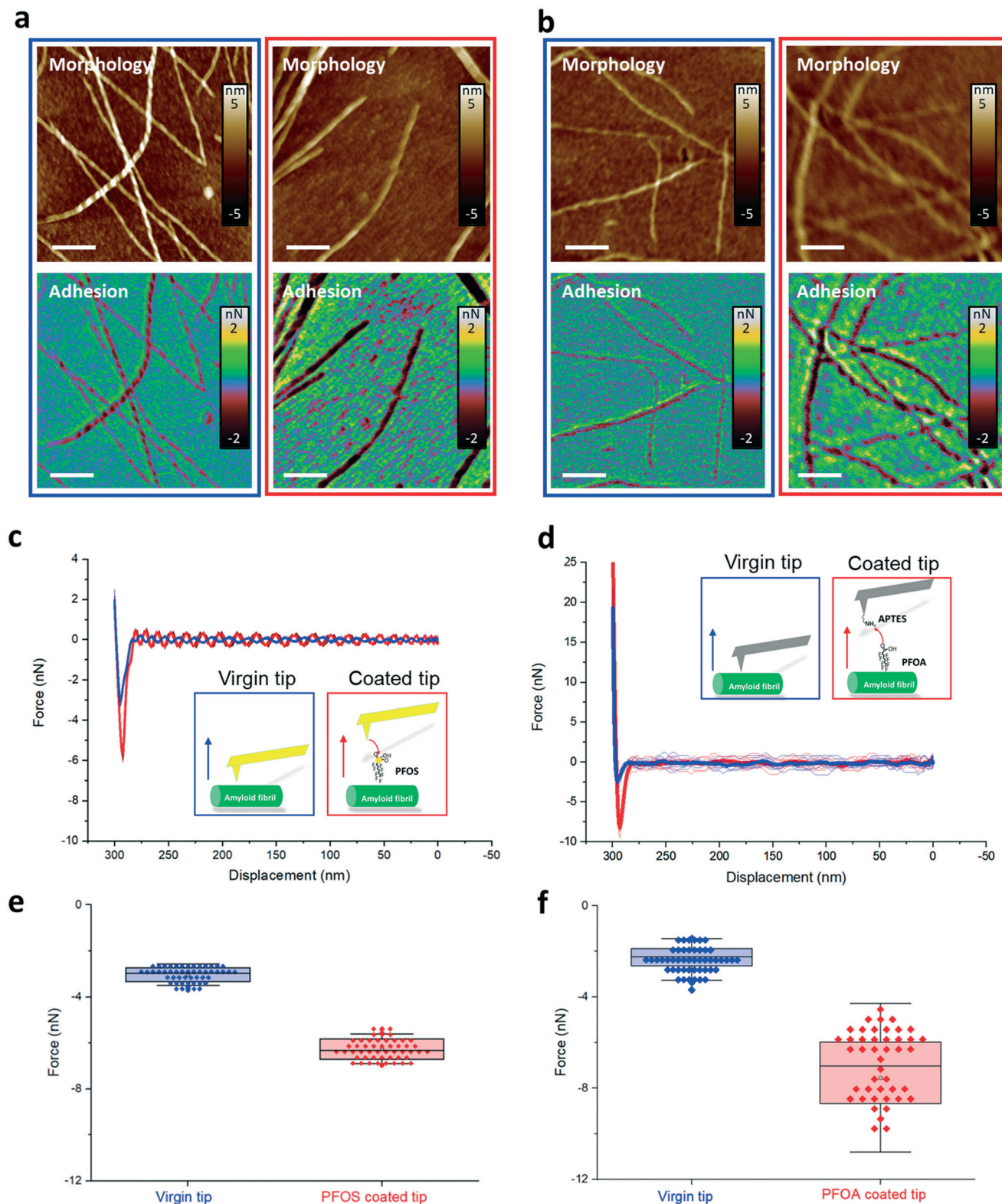


Fig. 4 Intermolecular adhesion force measurement by using AFM force spectroscopy. Blue boxes, curves, and dots show the results measured for virgin tips, whereas the red boxes, curves, and dots show the results measured for PFASs (PFOS or PFOA) coated tips. (a and b) AFM morphology of amyloid fibrils and adhesion force map of PFOS (a) and PFOA (b). Scale bar is 200 nm. (c and d) Adhesion–distance relationship between amyloid fibrils and virgin/coated tips: (c) PFOS coated tip and (d) PFOA coated tip; the bold lines are the average data summarized from 30 locations of amyloid fibrils. (e and f) The statistical data of adhesion force from 30 locations of amyloid fibrils on the adhesive map.



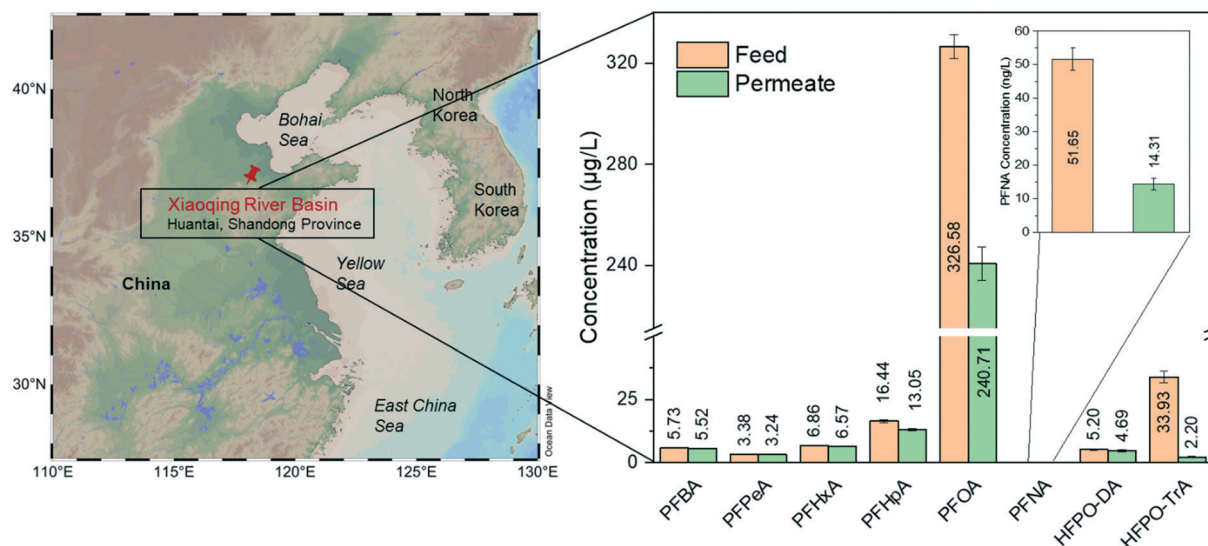


Fig. 5 Treatment of water sample from Xiaoqing River basin by AM membrane. The map is generated from Schlitzer, Reiner, Ocean Data View, odv.awi.de, 2020. The removal efficiencies are summarized in the ESI† (Table S4).

concentration of PFBA in the permeate reduced to 3.65 ng L⁻¹, which means that >96% of PFBA was removed by the amyloid-carbon hybrid membrane. It is worth noting that PFBA has the lowest MW among all the measured PFASs and is most difficult to remove as a member of the PFAS group. This could be mainly induced by its short chain length (3 CF₂ units in the molecule structure) and low hydrophobicity. Finally, except for PFBA, both the long- and short-chain PFASs were fully removed within the detection limits, which demonstrates unambiguously that the hybrid membrane has the capacity to adsorb a broad range of PFASs.

As an adsorbent for PFAS, activated carbon (AC) is investigated most frequently for comparing the treatment performance by other technologies.⁵⁶ Existing studies indicated that the performance of both commercial and novel developed AC depends on the PFAS chain length as well.^{50,57–59} In most cases, the AC removal efficiency for short-chain PFASs is low and falls into a wide range. For instance, Son *et al.* reported that 85% removal efficiency of

the short-chain PFASs (PFHxS) was reached at equilibrium, while for the others (PFPeA, PFHxA, PFHpA, PFBS) this was reached in the range of 13–55% for different powder-activated carbons (PACs).⁵⁷ The results from Zhang *et al.* showed that the removal efficiency of the mixed PFASs, including long-chain PFASs (PFOA and PFOS) and short-chain PFASs (PFBA and PFBS), was in the range of 5–75%.⁶⁰ Moreover, single use of granular activated carbon in treating real waters with co-contaminants or other natural organic matter can feature very low performance in the PFAS removal efficiency.⁵⁰

However, after introducing amyloid fibrils to the matrix of activated carbon, the removal efficiency reaches 96% in the worst case, emphasizing the unique capability of amyloid fibrils for binding with PFBA. In addition to all mechanisms mentioned before, this binding can be interpreted by the complex intermolecular binding events between amyloid fibrils and PFBA. Moreover, the addition of activated carbon is efficient and economical to improve the PFAS adsorption by the amyloid-carbon hybrid membrane, not only for its



Fig. 6 PFAS treatment by the amyloid-carbon hybrid membrane.

well-known absorption features but also because it provides a highly porous structure that leads to higher permeability and contact area with amyloid fibrils. These findings demonstrate unambiguously the synergistic effect of amyloids and activated carbon for PFAS-contaminated water treatment in a scalable and sustainable way.

Sustainability footprint

We compare the sustainability footprint of nanofiltration and amyloid-carbon hybrid membrane, as shown in Fig. 7. The details of the methodology of footprint analysis are added in the ESI† (Table S5). Nanofiltration, especially the commercial nanofiltration membrane, has been widely studied in PFAS treatment and is chosen here for the consideration of equilibration and practicality.^{47,61} The evaluation is simplified from our previous analysis published in *Chem. Soc. Rev.* 2019 (ref. 14) and including 8 aspects: two semi-qualitative aspects (environmental friendliness and public acceptability) and 6 aspects (long-chain PFAS removal efficiency, short-chain PFAS removal efficiency, OPEX, CAPEX, water recovery, and required

energy) with reference values. The performance of the technologies in each aspect is ranked as a low ($i = 1$), medium ($i = 2$), and high ($i = 3$) level score. This is a stochastic method and robust and simple enough to be generalized to additional or fewer characteristics, where the technologies can be sorted out differently, and characteristics can be adjusted more flexibly, by which the basic trade-off between the advantages and disadvantages of each technology can be evaluated.

Organic chemicals, such as dimethylacetamide (DMAc) and dimethylformamide (DMF), are widely used as solvents for polymeric membrane preparation. It is inevitable to dispose of these solvents during the membrane synthesis process. Improper treatment of the solvent residue may have negative impacts on the environment and human health. On the contrary, the amyloid-carbon hybrid membrane is prepared in water at any pH and only consists of activated carbon and amyloid fibrils, which ingeniously reduces the harm to the environment and humans. Moreover, the amyloid-carbon hybrid membrane shows great advantages in investment cost (CAPEX) since the industrial grade of BLG (whey, a bioproduct of the dairy industry) is much cheaper than the polymer-based

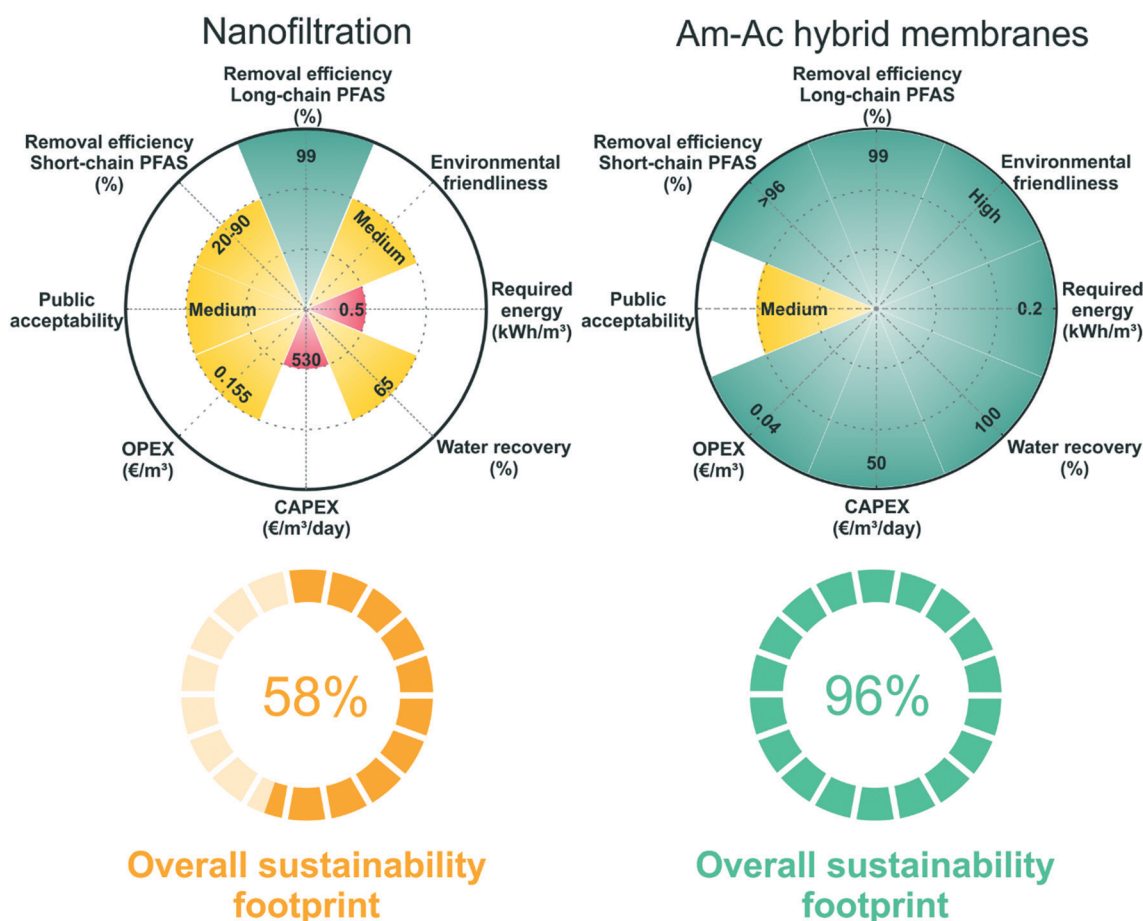


Fig. 7 Sustainability footprint comparison between nanofiltration and amyloid-carbon hybrid membrane. The aspects considered are long-chain PFAS removal efficiency, short-chain PFAS removal efficiency, public acceptability, OPEX, CAPEX, water recovery, required energy, and environmental friendliness. The performance of the technologies in each parameter is evaluated on a 3-rank basis of low (red), medium (yellow), and high (green) levels. The overall sustainability footprint of each technology is evaluated according to each aspect.



membranes. On the other hand, nanofiltration scores medium in most aspects due to its high operating cost (OPEX), relatively low water recovery, and lower short-chain PFAS removal efficiency than the amyloid-carbon hybrid membrane. From the environmental friendliness point of view, the amyloid-carbon hybrid membrane performs better than nanofiltration in fabrication, application, and energy consumption. For instance, the release of toxic organic solvents during the fabrication of polymeric membrane and high energy consumption during operation of nanofiltration increase the stress in the bearing capacity of the environment and further treatment processes, whilst protein dominant processes are solvent-free and energy saving.

Then we estimate the overall sustainability footprint by summing up the individual components as $100\% \cdot \sum_{j=1}^8 \left(\frac{i}{5}\right)^j \cdot \frac{1}{8}$, where each of the $j = 8$ factors carries a weight between 1/3 and 1 depending on the score i . The sustainability footprint for the amyloid-carbon hybrid membrane and nanofiltration was estimated at around 96% and 58%, respectively, which clearly reveals the superiority of the amyloid-carbon hybrid membrane over nanofiltration for PFAS removal in terms of sustainability and efficiency.

Conclusions

In summary, we have demonstrated that amyloid membranes can remove long-chain PFASs efficiently from the aqueous environment by adsorption mechanisms. The adsorption membrane performance can be dramatically enhanced under acidic conditions, which mainly exploits the electrostatic interactions between amyloid fibrils and PFASs. The isotherm curves of representative PFASs (PFOS and PFOA) show that the PFOS is easily adsorbed but has a lower adsorption capacity than PFOA. Further AFM adhesion force spectroscopy measurement firstly demonstrates that hydrophobic interactions have a significant role in PFAS adsorption onto the amyloid surface. The treatment of a real water sample proves again that the amyloid fibril works better for long-chain PFASs than short-chain ones. The performance towards the removal of low molecular weight PFASs can be enhanced by using the amyloid-carbon hybrid membrane, which also possesses higher permeability, removing all PFASs at a trace level of concentration. Finally, the comparison of the sustainability footprint reveals the superiority of the amyloid-carbon hybrid membrane over a commercial membrane process for PFAS removal. These results demonstrate that it should be easy to reach the scale-up of the treatment of PFAS contaminated water by amyloid-carbon hybrid membranes in a fully economical and sustainable way.

Conflicts of interest

RM and SB are inventors of an ETH-related patent. BluAct Technologies GmbH has an exclusive licence of this patent from ETH.

Acknowledgements

T. J. acknowledges the financial support from ETH Zurich and China Scholarship Council (Grant No. 201908320491).

References

- 1 F. M. Hekster, R. W. Laane and P. de Voegt, in *Rev. Environ. Contam. Toxicol.*, Springer, 2003, pp. 99–121.
- 2 M. H. B. Müller, A. Polder, O. Brynildsrud, R. Grønnestad, M. Karimi, E. Lie, W. B. Manyilizu, R. Mdegela, F. Mokiti and M. Murtadha, Prenatal exposure to persistent organic pollutants in Northern Tanzania and their distribution between breast milk, maternal blood, placenta and cord blood, *Environ. Res.*, 2019, **170**, 433–442.
- 3 C. Flores, F. Ventura, J. Martin-Alonso and J. Caixach, Occurrence of perfluorooctane sulfonate (PFOS) and perfluorooctanoate (PFOA) in N.E. Spanish surface waters and their removal in a drinking water treatment plant that combines conventional and advanced treatments in parallel lines, *Sci. Total Environ.*, 2013, **461–462**, 618–626.
- 4 Z. R. Hopkins, M. Sun, J. C. DeWitt and D. R. U. Knappe, Recently Detected Drinking Water Contaminants: GenX and Other Per- and Polyfluoroalkyl Ether Acids, *J. - Am. Water Works Assoc.*, 2018, **110**, 13–28.
- 5 P. Zhao, X. Xia, J. Dong, N. Xia, X. Jiang, Y. Li and Y. Zhu, Short-and long-chain perfluoroalkyl substances in the water, suspended particulate matter, and surface sediment of a turbid river, *Sci. Total Environ.*, 2016, **568**, 57–65.
- 6 R. Rattanaoudom and C. Visvanathan, Removal of PFOA by hybrid membrane filtration using PAC and hydrotalcite, *Desalin. Water Treat.*, 2011, **32**, 262–270.
- 7 D. Q. Zhang, W. L. Zhang and Y. N. Liang, Adsorption of perfluoroalkyl and polyfluoroalkyl substances (PFASs) from aqueous solution - A review, *Sci. Total Environ.*, 2019, **694**, 133606.
- 8 N. Kishimoto and M. Kobayashi, Effects of three additives on the removal of perfluorooctane sulfonate (PFOS) by coagulation using ferric chloride or aluminum sulfate, *Water Sci. Technol.*, 2016, **73**, 2971–2977.
- 9 Y. R. Dai, J. F. Niu, L. F. Yin, J. J. Xu and K. Sun, Enhanced sorption of perfluorooctane sulfonate (PFOS) on carbon nanotube-filled electrospun nanofibrous membranes, *Chemosphere*, 2013, **93**, 1593–1599.
- 10 M. Peydayesh, M. Pauchard, S. Bolisetty, F. Stellacci and R. Mezzenga, Ubiquitous aluminium contamination in water and amyloid hybrid membranes as a sustainable possible solution, *Chem. Commun.*, 2019, **55**, 11143–11146.
- 11 S. Bolisetty and R. Mezzenga, Amyloid-carbon hybrid membranes for universal water purification, *Nat. Nanotechnol.*, 2016, **11**, 365.
- 12 S. Bolisetty, N. Reinhold, C. Zeder, M. N. Orozco and R. Mezzenga, Efficient purification of arsenic-contaminated water using amyloid-carbon hybrid membranes, *Chem. Commun.*, 2017, **53**, 5714–5717.
- 13 S. Bolisetty, N. M. Coray, A. Palika, G. A. Prenosil and R. Mezzenga, Amyloid hybrid membranes for removal of



- clinical and nuclear radioactive wastewater, *Environ. Sci.: Water Res. Technol.*, 2020, **6**, 3249–3254.
- 14 S. Bolisetty, M. Peydayesh and R. Mezzenga, Sustainable technologies for water purification from heavy metals: review and analysis, *Chem. Soc. Rev.*, 2019, **48**, 463–487.
 - 15 M. Peydayesh and R. Mezzenga, Protein nanofibrils for next generation sustainable water purification, *Nat. Commun.*, 2021, **12**, 1–17.
 - 16 A. Palika, A. Rahimi, S. Bolisetty, S. Handschin, P. Fischer and R. Mezzenga, Amyloid hybrid membranes for bacterial & genetic material removal from water and their anti-biofouling properties, *Nanoscale Adv.*, 2020, **2**, 4665–4670.
 - 17 J.-M. Jung, G. Savin, M. Pouzot, C. Schmitt and R. Mezzenga, Structure of heat-induced β -lactoglobulin aggregates and their complexes with sodium-dodecyl sulfate, *Biomacromolecules*, 2008, **9**, 2477–2486.
 - 18 H. Joerss, C. Apel and R. Ebinghaus, Emerging per- and polyfluoroalkyl substances (PFASs) in surface water and sediment of the North and Baltic Seas, *Sci. Total Environ.*, 2019, **686**, 360–369.
 - 19 S. Swillens, Interpretation of binding curves obtained with high receptor concentrations: practical aid for computer analysis, *Mol. Pharmacol.*, 1995, **47**, 1197–1203.
 - 20 H. Motulsky, *The GraphPad guide to analyzing radioligand binding data*, GraphPad Software, Inc, 1996, 1–19.
 - 21 H. Oliveira, M. Rangl, A. Ebner, B. Mayer, P. Hinterdorfer and A. P. Pêgo, Molecular recognition force spectroscopy: a new tool to tailor targeted nanoparticles, *Small*, 2011, **7**, 1236–1241.
 - 22 J. Zhou, L. Venturelli, L. Keiser, S. K. Sekatskii, F. O. Gallaire, S. Kasas, G. Longo, T. P. Knowles, F. S. Ruggeri and G. Dietler, Environmental Control of Amyloid Polymorphism by Modulation of Hydrodynamic Stress, *ACS Nano*, 2020, **15**(1), 944–953.
 - 23 J. Zhou, F. S. Ruggeri, M. R. Zimmermann, G. Meisl, G. Longo, S. K. Sekatskii, T. P. Knowles and G. Dietler, Effects of sedimentation, microgravity, hydrodynamic mixing and air–water interface on α -synuclein amyloid formation, *Chem. Sci.*, 2020, **11**, 3687–3693.
 - 24 M. Park, S. Wu, I. J. Lopez, J. Y. Chang, T. Karanfil and S. A. Snyder, Adsorption of perfluoroalkyl substances (PFAS) in groundwater by granular activated carbons: Roles of hydrophobicity of PFAS and carbon characteristics, *Water Res.*, 2020, **170**, 115364.
 - 25 B. D. Turner, S. W. Sloan and G. R. Currell, Novel remediation of per- and polyfluoroalkyl substances (PFASs) from contaminated groundwater using Cannabis Sativa L. (hemp) protein powder, *Chemosphere*, 2019, **229**, 22–31.
 - 26 M. Zhao, J. Hu, H. Zhang, K. Nishinari and Y. Fang, Electrostatic complexation of β -lactoglobulin aggregates with κ -carrageenan and the resulting emulsifying and foaming properties, *J. Dairy Sci.*, 2020, **103**, 8709–8720.
 - 27 G. Lee, W. Lee, H. Lee, S. Woo Lee, D. Sung Yoon, K. Eom and T. Kwon, Mapping the surface charge distribution of amyloid fibril, *Appl. Phys. Lett.*, 2012, **101**, 043703.
 - 28 M. Usuelli, T. Germerdonk, Y. Cao, M. Peydayesh, M. Bagnani, S. Handschin, G. Nyström and R. Mezzenga, Polysaccharide-reinforced amyloid fibril hydrogels and aerogels, *Nanoscale*, 2021, **13**, 12534–12545.
 - 29 E. Steinle-Darling and M. Reinhard, Nanofiltration for Trace Organic Contaminant Removal: Structure, Solution, and Membrane Fouling Effects on the Rejection of Perfluorochemicals, *Environ. Sci. Technol.*, 2008, **42**, 5292–5297.
 - 30 C. C. Murray, H. Vatankhah, C. A. McDonough, A. Nickerson, T. T. Hedtke, T. Y. Cath, C. P. Higgins and C. L. Bellona, Removal of per- and polyfluoroalkyl substances using super-fine powder activated carbon and ceramic membrane filtration, *J. Hazard. Mater.*, 2019, **366**, 160–168.
 - 31 T. D. Appleman, C. P. Higgins, O. Quinones, B. J. Vanderford, C. Kolstad, J. C. Zeigler-Holady and E. R. V. Dickenson, Treatment of poly- and perfluoroalkyl substances in US full-scale water treatment systems, *Water Res.*, 2014, **51**, 246–255.
 - 32 F. Li, J. Duan, S. Tian, H. Ji, Y. Zhu, Z. Wei and D. Zhao, Short-chain per- and polyfluoroalkyl substances in aquatic systems: Occurrence, impacts and treatment, *Chem. Eng. J.*, 2020, **380**, 122506.
 - 33 M. Ateia, A. Alsaiee, T. Karanfil and W. Dichtel, Efficient PFAS Removal by Amine-Functionalized Sorbents: Critical Review of the Current Literature, *Environ. Sci. Technol. Lett.*, 2019, **6**, 688–695.
 - 34 B. Ji, P. Kang, T. Wei and Y. Zhao, Challenges of aqueous per- and polyfluoroalkyl substances (PFASs) and their foreseeable removal strategies, *Chemosphere*, 2020, 126316.
 - 35 Y. Pan, H. Zhang, Q. Cui, N. Sheng, L. W. Yeung, Y. Guo, Y. Sun and J. Dai, First report on the occurrence and bioaccumulation of hexafluoropropylene oxide trimer acid: an emerging concern, *Environ. Sci. Technol.*, 2017, **51**, 9553–9560.
 - 36 Y. Bao, S. Deng, X. Jiang, Y. Qu, Y. He, L. Liu, Q. Chai, M. Mumtaz, J. Huang and G. Cagnetta, Degradation of PFOA substitute: GenX (HFPO–DA ammonium salt): oxidation with UV/persulfate or reduction with UV/sulfite?, *Environ. Sci. Technol.*, 2018, **52**, 11728–11734.
 - 37 X. Song, R. Vestergren, Y. Shi, J. Huang and Y. Cai, Emissions, transport, and fate of emerging per- and polyfluoroalkyl substances from one of the major fluoropolymer manufacturing facilities in China, *Environ. Sci. Technol.*, 2018, **52**, 9694–9703.
 - 38 C. Zhang, H. Yan, F. Li, X. Hu and Q. Zhou, Sorption of short- and long-chain perfluoroalkyl surfactants on sewage sludges, *J. Hazard. Mater.*, 2013, **260**, 689–699.
 - 39 M. Peydayesh, S. Bolisetty, T. Mohammadi and R. Mezzenga, Assessing the binding performance of amyloid–carbon membranes toward heavy metal ions, *Langmuir*, 2019, **35**, 4161–4170.
 - 40 I. Medalsy, U. Hensen and D. J. Muller, Imaging and Quantifying Chemical and Physical Properties of Native Proteins at Molecular Resolution by Force–Volume AFM, *Angew. Chem., Int. Ed.*, 2011, **50**, 12103–12108.
 - 41 A. Borgia, P. M. Williams and J. Clarke, Single-Molecule Studies of Protein Folding, *Annu. Rev. Biochem.*, 2008, **77**, 101–125.



- 42 S. Lee and M. Elimelech, Relating organic fouling of reverse osmosis membranes to intermolecular adhesion forces, *Environ. Sci. Technol.*, 2006, **40**, 980–987.
- 43 Q. Li and M. Elimelech, Organic fouling and chemical cleaning of nanofiltration membranes: measurements and mechanisms, *Environ. Sci. Technol.*, 2004, **38**, 4683–4693.
- 44 H. Joerss, T.-R. Schramm, L. Sun, C. Guo, J. Tang and R. Ebinghaus, Per- and polyfluoroalkyl substances in Chinese and German river water – Point source- and country-specific fingerprints including unknown precursors, *Environ. Pollut.*, 2020, **267**, 115567.
- 45 C. Zhao, T. Zhang, G. Hu, J. Ma, R. Song and J. Li, Efficient removal of perfluorooctane sulphonate by nanofiltration: Insights into the effect and mechanism of coexisting inorganic ions and humic acid, *J. Membr. Sci.*, 2020, **610**, 118176.
- 46 C. W. Zhao, C. Y. Tang, P. Li, P. Adrian and G. S. Hu, Perfluorooctane sulfonate removal by nanofiltration membrane-the effect and interaction of magnesium ion/humic acid, *J. Membr. Sci.*, 2016, **503**, 31–41.
- 47 J. X. Wang, L. Wang, C. Q. Xu, R. Zhi, R. Miao, T. Liang, X. L. Yue, Y. T. Lv and T. T. Liu, Perfluorooctane sulfonate and perfluorobutane sulfonate removal from water by nanofiltration membrane: The roles of solute concentration, ionic strength, and macromolecular organic foulants, *Chem. Eng. J.*, 2018, **332**, 787–797.
- 48 C. Y. Tang, Q. S. Fu, C. S. Criddle and J. O. Leckie, Effect of flux (transmembrane pressure) and membrane properties on fouling and rejection of reverse osmosis and nanofiltration membranes treating perfluorooctane sulfonate containing wastewater, *Environ. Sci. Technol.*, 2007, **41**, 2008–2014.
- 49 Á. Soriano, D. Gorri and A. Urriaga, Selection of High Flux Membrane for the Effective Removal of Short-Chain Perfluorocarboxylic Acids, *Ind. Eng. Chem. Res.*, 2019, **58**, 3329–3338.
- 50 I. Ross, J. McDonough, J. Miles, P. Storch, P. T. Kochunaryanan, E. Kalve, J. Hurst, S. S. Dasgupta and J. Burdick, A review of emerging technologies for remediation of PFASs, *Remediation*, 2018, **28**, 101–126.
- 51 E. Gagliano, M. Sgroi, P. P. Falciglia, F. G. A. Vagliasindi and P. Roccaro, Removal of poly- and perfluoroalkyl substances (PFAS) from water by adsorption: Role of PFAS chain length, effect of organic matter and challenges in adsorbent regeneration, *Water Res.*, 2020, **171**, 115381.
- 52 D. Kupryianchyk, S. E. Hale, G. D. Breedveld and G. Cornelissen, Treatment of sites contaminated with perfluorinated compounds using biochar amendment, *Chemosphere*, 2016, **142**, 35–40.
- 53 M. Ateia, A. Maroli, N. Tharayil and T. Karanfil, The overlooked short-and ultrashort-chain poly-and perfluorinated substances: A review, *Chemosphere*, 2019, **220**, 866–882.
- 54 Q. Zhang, S. Bolisetty, Y. Cao, S. Handschin, J. Adameik, Q. Peng and R. Mezzenga, Selective and efficient removal of fluoride from water: in situ engineered amyloid fibril/ZrO₂ hybrid membranes, *Angew. Chem., Int. Ed.*, 2019, **58**, 6012–6016.
- 55 M. Peydayesh, M. K. Suter, S. Bolisetty, S. Boulos, S. Handschin, L. Nyström and R. Mezzenga, Amyloid fibrils aerogel for sustainable removal of organic contaminants from water, *Adv. Mater.*, 2020, **32**, 1907932.
- 56 I. M. Militao, F. A. Roddick, R. N. Bergamasco and L. Fan, Removing PFAS from aquatic systems using natural and renewable material-based adsorbents: A review, *J. Environ. Chem. Eng.*, 2021, 105271.
- 57 H. Son, T. Kim, H.-S. Yoom, D. Zhao and B. An, The Adsorption Selectivity of Short and Long Per-and Polyfluoroalkyl Substances (PFASs) from Surface Water Using Powder-Activated Carbon, *Water*, 2020, **12**, 3287.
- 58 P. McCleaf, S. Englund, A. Östlund, K. Lindegren, K. Wiberg and L. Ahrens, Removal efficiency of multiple poly- and perfluoroalkyl substances (PFASs) in drinking water using granular activated carbon (GAC) and anion exchange (AE) column tests, *Water Res.*, 2017, **120**, 77–87.
- 59 M. C. Hansen, M. H. Børresen, M. Schlabach and G. Cornelissen, Sorption of perfluorinated compounds from contaminated water to activated carbon, *J. Soils Sediments*, 2010, **10**, 179–185.
- 60 D. Zhang, Q. He, M. Wang, W. Zhang and Y. Liang, Sorption of perfluoroalkylated substances (PFASs) onto granular activated carbon and biochar, *Environ. Technol.*, 2021, **42**, 1798–1809.
- 61 M. Li, F. Sun, W. Shang, X. Zhang, W. Dong, Z. Dong and S. Zhao, Removal mechanisms of perfluorinated compounds (PFCs) by nanofiltration: Roles of membrane-contaminant interactions, *Chem. Eng. J.*, 2021, **406**, 126814.

